Two balls in one dimension with gravity

N. D. Whelan,* D. A. Goodings, and J. K. Cannizzo†
Physics Department, McMaster University, Hamilton, Ontario, Canada L8S 4M1
(Received 16 October 1989)

A study is reported of a simple dynamical system with two degrees of freedom having discontinuities due to collisions. It consists of two point masses or balls constrained to move in one dimension above a floor in a constant gravitational field. All collisions are assumed to be elastic. When the ratio r of the upper mass to the lower mass is less than unity the motion is chaotic almost everywhere. On the other hand, when $r > 1$ the motion shows typical Kolmogorov-Arnol'd-Moser behavior with quasiperiodic and chaotic trajectories coexisting in the phase space. It is shown that for particular values of the mass ratio, denoted by r_n, a sequence of n rapid ball-ball collisions close to the floor has the net effect of reversing the velocities of both balls. This demonstration leads to the identification of families of stable and unstable fixed points of the Poincaré section, which to a considerable extent determine the overall structure of the map. By means of a method due to Lorenz, the largest Lyapunov exponent λ_1 has been calculated for many values of the mass ratio and for a variety of trajectories. For chaotic trajectories, a plot of λ_1 as a function of r is found to have local minima at the values r_n corresponding to velocity-reversing collision sequences. This is thought to result from the fact that when $r = r_n$ the chaotic trajectories lie in many isolated regions of the phase space, whereas when r is different from any of the r_n, the chaotic regions merge to form a single region of global chaos.

I. INTRODUCTION

Despite their relative simplicity, Hamiltonian systems with two degrees of freedom, such as two coupled nonlinear oscillators, give rise to very complex behavior. A well-known example of such a system is the Hénon-Heiles Hamiltonian[1] for which the position coordinates and the momenta show a transition from quasiperiodic motion at low energies to almost completely chaotic motion at higher energies, with both types of behavior coexisting at intermediate energies. The general features of this transition may be understood on the basis of the Kolmogorov-Arnol'd-Moser (KAM) theorem. The physical content of this theory has been well described by a number of authors.[2–6]

While the flow induced by coupled-oscillator systems is generally continuous and differentiable, there is another class of Hamiltonian systems for which the flow is piecewise continuous with discontinuities in the momenta resulting from collisions. In this general class there are some systems which do not exhibit quasiperiodic behavior. The most physically interesting example is the gas of n-dimensional hard spheres with elastic collisions which Sinai[7,8] has shown to be ergodic and mixing for $n = 2$ and to have (possibly many) ergodic components of positive measure and positive entropy for $n > 2$. There are also dynamical systems with discontinuities in which both quasiperiodic and chaotic motions are known to coexist. A classic example is the simplified model of cosmic ray acceleration developed by Fermi, Pasta, and Ulam in which a point mass moves between two walls, one fixed and one oscillating.[9] Another example is the motion of a billiard inside a plane convex region, sometimes referred to as the stadium problem.[10] Recently, Lehtihet and Miller[11] have reported a numerical study of a billiard confined to a symmetric wedge-shaped region in a constant gravitational field. These examples all show typical KAM behavior despite the fact that the equations of motion of the point mass are strictly linear. Clearly the collisions themselves are equivalent to the action of nonlinear forces.

Mathematical studies of dynamical systems with singularities caused by collisions have been carried out by Wojtkowski[12–14] and by Katok and Strelcyn.[15] The latter authors have extended to a broad class of such systems the theory of Pesin[16] relating the ergodic properties of a system to its Lyapunov exponents. The billiard inside a plane convex region has been studied by Wojtkowski,[12] who has established conditions on the shape of the boundary which lead to nonzero Lyapunov exponents and strong mixing properties. Very recently Wojtkowski[14] studied a system of balls confined to one dimension above a floor in a constant gravitational field, all collisions being assumed to be elastic. For the case in which the masses decrease monotonically with height, he established the existence of at least one nonzero Lyapunov exponent for almost all trajectories in the phase space.

The present paper is an exploration of the physics of a simple dynamical system with singularities caused by collisions. The system consists of two point masses—we think of them as balls—constrained to move vertically in one dimension under the influence of a constant gravitational field. In addition to conserving momentum, the collisions between the balls are assumed to be elastic. Furthermore, when the lower ball collides with the floor, taken to be at $x = 0$, its velocity is simply reversed in direction. Except for the instants when collisions occur,

the system is described by the Hamiltonian,

$$H=\frac{p_1^2}{2m_1}+\frac{p_2^2}{2m_2}+m_1gx_1+m_2gx_2\ , \tag{1}$$

where g is the acceleration due to gravity, and m_1 and m_2 are the masses of the balls. If x_1 denotes the position of the lower ball, the motion is constrained by the conditions $x_1 \geq 0$, $x_2 \geq x_1$.

Our system with two degrees of freedom is the simplest nontrivial case of Wojtkowski's system of one-dimensional balls.[14] In the appendix of his paper, Wojtkowski shows that this system is related by a canonical transformation to the billiard in the symmetric wedge studied by Lehtihet and Miller[11]—a demonstration that is particularly interesting in the light of the fact that from a physical point of view the two systems behave quite differently. As the dynamical behavior of the two-ball system is easy to comprehend, we believe the present work complements Lehtihet and Miller's paper while showing certain similarities in the structure of the results.

The plan of the paper is as follows. After defining suitable dimensionless variables and Poincaré maps in Sec. II, we examine the simple fixed points of the two-ball system in Sec. III. In Sec. IV it is shown that for particular values of the mass ratio r_n a sequence of rapid collisions near $x=0$ can effectively reverse the velocities of both balls. This leads to identifying families of stable and unstable fixed points, described in Sec. V. It is shown in Sec. VI that these fixed points largely determine the structure of the Poincaré maps. The motion of the system in the limit of large r is studied in Sec. VII, leading to a demonstration that the fraction of the accessible area of the Poincaré map occupied by chaotic trajectories is proportional to $r^{-1/2}$. This supports our belief that the integrable case corresponds to the limit of infinite r. In Sec. VIII we describe the results of calculations of the Lyapunov exponents for chaotic trajectories as a function of r. The structure of these plots is interpreted in terms of the suppression of chaos at the values r_n associated with velocity-reversing collision sequences. Concluding remarks are contained in Sec. IX.

One of the objectives of the present work is to show that the physical behavior of the simple two-ball system with discontinuities is intimately related to the mathematical structure of its fixed points. One might even argue that it is this structure which ultimately determines the characteristics of the dynamical motion.

II. PRELIMINARY DETAILS

Because the constant-acceleration equations for a particle moving in a uniform gravitational field are independent of its mass, we have found it convenient to use position and velocity instead of the usual canonical variables. It is also useful to introduce the following dimensionless variables:

$$\begin{aligned} x' &= (mg/E)x\ , \\ v' &= (m/E)^{1/2}v\ , \\ t' &= (m/E)^{1/2}gt\ , \end{aligned} \tag{2}$$

where $m=m_1+m_2$, E is the total energy of the system, and g is the acceleration due to gravity. In terms of these variables the usual constant-acceleration equations are

$$\begin{aligned} v' &= v_0'-t'\ , \\ x' &= x_0'+v_0't'-\tfrac{1}{2}t'^2\ , \\ v'^2 &= v_0'^2-2(x'-x_0')\ . \end{aligned} \tag{3}$$

This is equivalent to setting $g=1$. Furthermore, if we define the dimensionless masses $m_1'=m_1/m=1/(r+1)$ and $m_2'=m_2/m=r/(r+1)$, the equation expressing conservation of energy takes the form

$$\tfrac{1}{2}m_1'v_1'^2+\tfrac{1}{2}m_2'v_2'^2+m_1'x_1'+m_2'x_2'=1\ . \tag{4}$$

Throughout the rest of the paper the primes will be omitted and x, v, t, m_1, and m_2 will denote these dimensionless variables.

It is well known that a dynamical system with two degrees of freedom can be reduced to the study of a two-dimensional area-preserving map. A suitable map of this kind in the present problem is the Poincaré section of v_2 plotted against x_2 at each instant that the lower ball hits the floor. For brevity we call this the $x_1=0$ Poincaré map. A slightly different map is the Poincaré plot of v_2 against x_2 at each instant that the balls collide. This will be called the ball-ball collision (BBC) map or BBC Poincaré map.

An example of an $x_1=0$ Poincaré map is shown in Fig. 1 for the case $r=0.5$. The parabolic boundary of this plot is approached when the upper ball has nearly all the energy of the system while the lower ball makes many low bounces against the floor. All the points in Fig. 1 arise from a single trajectory, and it is noteworthy that they appear to be distributed uniformly inside the parabolic boundary. Behavior of this kind is found for almost any initial conditions, indicating that the motion is ergodic. This is consistent with Wojtkowski's theorem[14]

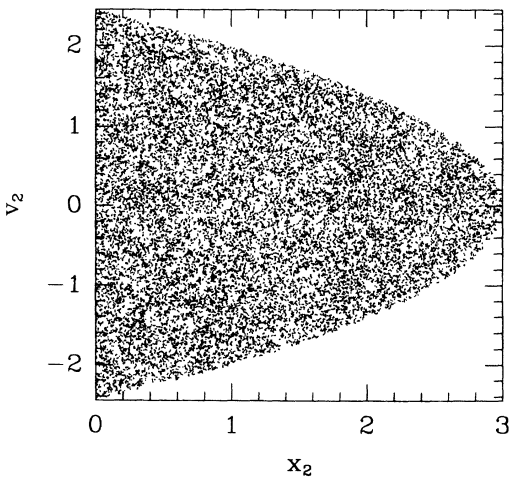

FIG. 1. $x_1=0$ Poincaré section for $r=0.5$ calculated using 15 000 points. Initial values: $x_c=0.28$, $v_{1c}=-1.2$, $v_{2c}=1.2$.

that when $r<1$ there is at least one nonzero Lyapunov exponent almost everywhere in the phase space.

In Fig. 2 we show the $x_1=0$ Poincaré section for $r=6$. (How this figure was calculated will be described in Sec. VI.) This plot is fairly typical of the general behavior found when $r>1$. In the central part of the plot one finds that the points generated by a single trajectory lie on a continuous closed curve, and the associated behavior of the system is quasiperiodic. Within the outermost closed curve is a group of nine islands belonging to a single trajectory, the associated behavior of the system again being quasiperiodic. Inside the nine islands there are fixed points constituting a 9-cycle (defined in Sec. III). The behavior of the system for this special trajectory is exactly periodic. Surrounding the outermost closed curve there is a broad chaotic region, the points of which were generated by a single trajectory. A prominent feature of this region is the set of three "bumps" ranged along the v_2 axis. Finally, within this chaotic region is a set of five large islands and another set of six smaller islands, two of which (on the sides of the parabola) are not easily discernible. These features—the central family of closed curves, the numerous island chains, and the broad chaotic region with several bumps—are common to all the Poincaré plots for r greater than about 3. It is these features that we wish to explain in mathematical and physical terms.

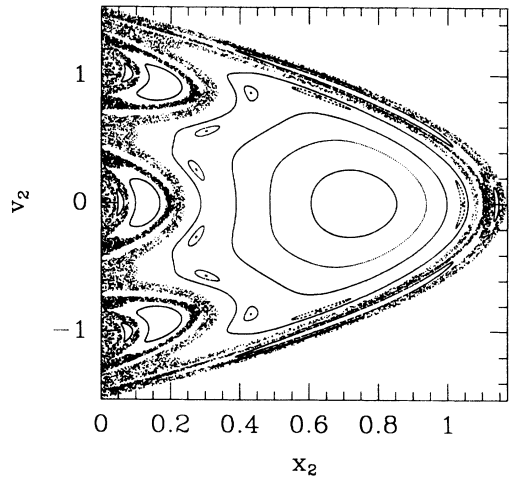

FIG. 2. $x_1=0$ Poincaré section for $r=6$, calculated as described in Sec. VI.

Greene[17] has argued that the structure of a two-dimensional area-preserving map may be understood in terms of its fixed points and their stability. Accordingly, in the following section we examine the fixed points of the ball-ball collision map.

III. FIXED POINTS OF THE BALL-BALL COLLISION MAP

Let ξ_i denote the vector (x_c, v_{1c}, v_{2c}) immediately before the ith ball-ball collision. Then if T is the map from one BBC to the next, we can write

$$\xi_{i+1}=T\xi_i \ . \tag{5}$$

A fixed point of the map satisfies $\bar{\xi}=T\bar{\xi}$.

In the two-ball system we have found that for every value of the mass ratio r there exists a simple fixed point $\bar{\xi}=(\bar{x}_c,\bar{v}_{1c},\bar{v}_{2c})$ such that during the time that the upper ball rises to its maximum height and falls back to $\bar{x}_c$, the lower ball makes a single collision with the floor and returns to $\bar{x}_c$. It is not difficult to show using Eq. (4) together with conservation of momentum in the collision that, just before the collision,

$$\bar{x}_c=\frac{2r+1}{3r+1} \ ,$$
$$\bar{v}_{1c}=r\left[\frac{2}{3r+1}\right]^{1/2} \ , \tag{6}$$
$$\bar{v}_{2c}=-\left[\frac{2}{3r+1}\right]^{1/2} \ .$$

This leads to a fixed point in the $x_1=0$ Poincaré section at $\bar{x}_2=2(r+1)/(3r+1)$, $\bar{v}_2=0$.

For this simple fixed point one can calculate explicitly the Jacobian matrix J as a function of r. The result is

$$J(\bar{\xi})=\frac{1}{(r+1)^2}\begin{bmatrix} r^2+1 & 2\bar{v}_{1c} & -2(r+1)\bar{v}_{1c} \\ 2r(2r-1)/\bar{v}_{1c} & r^2-4r+1 & 2(r^2-1) \\ 2r(r-2)/\bar{v}_{1c} & -2(2r-1) & r^2-2r-3 \end{bmatrix} \ . \tag{7}$$

The eigenvalues of this matrix determine the nature of the stability of the fixed point. For all values of r there is one eigenvalue equal to unity while the other two eigenvalues are the roots of the equation

$$y^2-2\frac{(r^2-4r-1)}{(r+1)^2}y+1=0 \ . \tag{8}$$

The discriminant of this equation is

$$d=\frac{16r(3r+1)(1-r)}{(r+1)^4} \ , \tag{9}$$

which is positive for $0<r<1$ and vanishes at $r=0$ and 1. For r in this range the modulus of one of the eigenvalues is always greater than unity, implying that $\bar{\xi}$ is a hyperbolic fixed point. This means that a trajectory starting from initial values close to those given by Eq. (6) will rapidly move away from the fixed point of the $x_1=0$ Poincaré map. One expects to find chaotic trajectories in this case, as in Fig. 1. For the case $r>1$ the eigenvalues are complex with unit modulus, implying that $\bar{\xi}$ is an elliptic fixed point. Thus, if the system starts out from initial

values close to those given by Eq. (6), the subsequent motion will be quasiperiodic, resulting in points in the Poincaré section lying on regular closed curves. This behavior is exactly what is found for the central family of closed curves in Fig. 2, in the middle of which lies the fixed point of Eq. (6).

In addition to the simple fixed point $\bar{\xi}$ there exist, for suitable values of the mass ratio, fixed points corresponding to m bounces of the lower ball from the floor between each ball-ball collision. It is not difficult to show that the corresponding values of $\bar{x}_c$, $\bar{v}_{1c}$, and $\bar{v}_{2c}$ are

$$\begin{aligned} &\bar{x}_c=\beta_m^2[1+2r-(m^2-1)r^2]\ , \\ &\bar{v}_{1c}=-r\sqrt{2}\beta_m m,\quad \bar{v}_{2c}=\sqrt{2}\beta_m m\ , \end{aligned} \tag{10}$$

where

$$\beta_m=[1+(m^2+2)r-(m^2-1)r^2]^{-1/2}\ . \tag{11}$$

For $m\geq 2$, the above expression for $\bar{x}_c$ is positive if $r<1/(m-1)$, implying that the fixed point corresponding to m bounces of the lower ball exists only if $0<r<1/(m-1)$. Although we have not found an expression for the Jacobian at these fixed points, they are almost certainly hyperbolic.

Apart from the fixed points of the map T, there exist fixed points of the map T^n for integer values of n. If $\bar{\xi}_1$ is a fixed point of T^n, then starting from $\bar{\xi}_1$ and repeatedly applying the map T, one generates a sequence of $n-1$ additional fixed points $\bar{\xi}_2,\ldots\bar{\xi}_n$ of T^n such that

$$\begin{aligned} &\bar{\xi}_{i+1}=T\bar{\xi}_i,\quad i=1,\ldots n-1 \\ &\bar{\xi}_1=T\bar{\xi}_n\ . \end{aligned} \tag{12}$$

These points define a periodic orbit of period n, also called an n-cycle. The set of points $\{\bar{\xi}_i\}$ is either stable (elliptic fixed points) or unstable (hyperbolic fixed points) since the trajectory which they define has one character or the other.

An example of a stable periodic orbit of period 9 is shown in Fig. 2 for the case $r=6$, generated by the (approximate) initial values $\bar{x}_c=0.2950$, $\bar{v}_{1c}=-1.9467$, and $\bar{v}_{2c}=1.0067$. If one follows the points as they are generated in the $x_1=0$ Poincaré section, one finds that they move in a clockwise direction around the central fixed point, requiring two circuits to return to the original point. Greene[17] has shown that in a two-dimensional area-preserving map such as that of Fig. 2, isolated fixed points may be identified by their rotation number P/Q, where P is the number of rotations around the central fixed point when going from a fixed point to its image though all Q members of the family. According to this definition, the 9-cycle of Fig. 2 can be identified with the rotation number 2/9. If any of the initial values is changed from the above values for $\bar{x}_c$, $\bar{v}_{1c}$, and $\bar{v}_{2c}$, the nine points become islands such as those shown in Fig. 2, and the motion of the system changes from periodic to quasiperiodic.

IV. COLLISION SEQUENCES NEAR $x=0$

In attempting to explain the structure lying close to the v_2 axis in plots like Fig. 2, we have discovered interesting families of fixed points which occur for special values of the mass ratio r. It turns out that these values of r, which are derived below, lie close to the locations of minima in the largest Lyapunov exponent calculated as a function of r for chaotic trajectories (Figs. 8 and 9). This will be discussed in Sec. VIII.

We consider a situation in which the upper ball has almost all the total energy of the system. While it rises to a maximum height and falls back to the vicinity of the floor, the lower ball, which has little energy, makes several low bounces on the floor. When the upper ball in its downward motion encounters the lower ball somewhere near the floor, it initiates a sequence of rapidly occurring ball-ball and floor-ball collisions which have the net effect of reversing the velocity of the upper ball. Under the right conditions the upper ball will emerge from the collision sequence with nearly all the energy of the system and the process will continue indefinitely.

To determine the values of r which enable this kind of periodic or quasiperiodic behavior to occur, consider the map which takes the velocities (v_1,v_2) just before a BBC to the velocities (w_1,w_2) immediately after it. Conservation of momentum and kinetic energy in the collision leads to

$$\begin{pmatrix} w_1 \\ w_2 \end{pmatrix}=\frac{1}{r+1}\begin{pmatrix} 1-r & 2r \\ 2 & r-1 \end{pmatrix}\begin{pmatrix} v_1 \\ v_2 \end{pmatrix}\ . \tag{13}$$

If this collision occurs very close to the floor, it will be followed almost immediately by a collision between the lower ball and the floor which changes w_1 to $-w_1$. Ignoring the change in the ball velocities caused by the gravitational acceleration during the short-time interval between one BBC and the next, we obtain the following matrix mapping the velocities (v_1,v_2) from one BBC to the next:

$$M=\frac{1}{r+1}\begin{pmatrix} r-1 & -2r \\ 2 & r-1 \end{pmatrix}\ . \tag{14}$$

Now let us assume that the collision sequence near $x=0$ has exactly n BBC's, at the end of which the velocities of the two balls are equal in magnitude but reversed in sign from what they were at the start of the collision sequence. This means that M^n has an eigenvalue equal to -1. With the help of energy conservation (and excepting the case $n=1$) this implies that $M^n=-I$ where I is the 2×2 unit matrix. Denoting the two eigenvalues of M by γ_+ and γ_-, it follows that $\gamma_\pm^n=-1$. Expressing γ_+ and γ_- in terms of r we find

$$\begin{aligned} &\gamma_\pm=\frac{r-1\pm i2\sqrt{r}}{r+1}=\exp(\pm i\phi)\ , \\ &\phi=\arctan[2\sqrt{r}\,/(r-1)]\ . \end{aligned} \tag{15}$$

Finally, setting $\exp(\pm in\phi)=\exp(\pm i\pi)$ and solving for r we obtain,

$$r_n=\cot^2(\pi/2n)\ . \tag{16}$$

TABLE I. Values of r_n from Eq. (16).

n	r_n	n	r_n	n	r_n	n	r_n
1	0.000	6	13.93	11	48.37	16	103.09
2	1.000	7	19.20	12	57.70	17	116.46
3	3.000	8	25.27	13	67.83	18	130.65
4	5.828	9	32.16	14	78.77	19	145.64
5	9.472	10	39.86	15	90.52	20	161.45

The numerical values of r_n for n up to 20 are given in Table I. (Note that solutions of $\exp(\pm in\phi)=\exp[\pm i(2p-1)\pi]$ corresponding to $p=2,3,\ldots$ are not of physical interest: instead of giving n collisions close to the floor, the upper ball acquires an upward velocity $v_2>v_1$ after approximately $n/(2p-1)$ collisions and the mapping of Eq. (14) no longer applies.) In view of (16) it is not surprising that the relation $r=\cot^2\theta$ gives the correspondence between the mass ratio r of the two-ball system and the semiangle θ of the billiard in the symmetric wedge studied by Lehtihet and Miller.[11] This will be discussed further in Sec. IX.

To sum up, if r is equal to r_n and if the state of the system is (x_c,v_1,v_2) going into the first BBC of the collision sequence, with $|v_2|$ large, x_c very small, and $|v_1|<|v_2|$, then the system will emerge from the collision sequence in the state $(x_c',-v_1,-v_2)$. Note that provided it is a good approximation to take the ball velocities to be constant between one collision and the next during the collision sequence, x_c' will be very close to x_c in accord with energy conservation. It is evident that in this special situation with r equal to r_n there is essentially no loss of information during the collision sequence; v_1 and v_2 are simply reversed in sign. We believe this provides a plausible explanation of why the Lyapunov exponent $\tilde{\lambda}_1$ calculated for chaotic trajectories as a function of r displays minima at the values r_n given in Table I. This will be discussed in more detail in Sec. VIII.

V. FAMILIES OF FIXED POINTS ASSOCIATED WITH VELOCITY REVERSALS

The preceding analysis leads to a description of families of fixed points associated with the velocity-reversing collision sequence for r equal to r_n. In what follows we shall assume that $r=r_n$ and that the collision sequence consisting of n BBC's occurs near $x=0$ with $|v_1|$ initially small. While not required by the velocity-reversal argument, the assumption that $|v_1|$ is small at the beginning and end of the collision sequence ensures that the next BBC (initiating the next collision sequence) will occur near $x=0$.

As before, let T be the map from one BBC to the next. It is clear from above that T^n maps (x_c,v_1,v_2) to a nearby point (x_c',v_1',v_2') in the phase space. Our primary interest is in sets of fixed points of the type defined in Eq. (12) for the map T^n.

Consider the fixed point of T^n corresponding to the first BBC of the collision sequence. Suppose that $v_1=0$ and x_c is small but nonzero going into the first collision. Then at the end of the collision sequence we will have, to a good approximation, the same value of x_c as at the beginning and $v_1=0$, $v_2=[2(1-x_c)(r+1)/r]^{1/2}$. Now suppose that during the time interval τ_2 between the end of the collision sequence and the first BBC of the next collision sequence the lower ball makes exactly m bounces, each of period τ_1. It is not difficult to show that the condition $\tau_2=m\tau_1$ leads to the following fixed point (in which v_1 and v_2 are the velocities just before the first collision of the collision sequence):

$$x_c=\frac{r_n+1}{m^2r_n+r_n+1}\ ,$$
$$v_1=0,\quad v_2=-\left[\frac{2m^2(r_n+1)}{m^2r_n+r_n+1}\right]^{1/2}\ , \tag{17}$$

where m is an integer large enough to make $x_c\ll 1$. Because of the approximation of constant ball velocities between collisions of the collision sequence, which is involved in the derivation of Eq. (17), these values do not locate the fixed points precisely. However, the error will decrease as m increases.

It will be seen in Sec. VI that Eq. (17) generates island chains having the fixed points in their interiors. [For the case $r_3=3.00$ this is true even for as small a value of m as $m=2$, showing that it is not essential to have $x_c\ll 1$ for (17) to be meaningful.] Clearly there is an infinite number of such fixed points corresponding to the integer values of m. Furthermore, each of these fixed points gives rise to a periodic orbit of period n. It may be noted that, for given n and m, while the upper ball executes one complete cycle (a complete up and down motion), the lower ball executes $m+n-1$ complete cycles. If angle variables are introduced to describe these two oscillatory motions, one can think of the motion occurring on a torus with winding number $\alpha(n,m)=m+n-1$.

It is interesting to consider the stability of the fixed points specified by Eq. (17). For given n and m, Eq. (17) gives the approximate location of a fixed point of T^n. It is easy to show from the equations of motion that a small departure δv_1 from $v_1=0$ induces changes in x_c and v_2 going as δv_1^2. Similarly, the change in τ_1 (defined above) is of order δv_1^2. Hence, to first order in δv_1, there is no change in τ_1, x_c, or v_2. If one uses this special feature of (17) and the velocity-reversing property of the collision sequence near $x=0$, and if one also uses the fact that the determinant of the Jacobian is unity, one can show that one of the eigenvalues of the Jacobian at the fixed point (17) of T^n is -1 while the product of the other two is -1. But since one eigenvalue must be unity (corresponding to the zero-valued Lyapunov exponent along the trajectory of the n fixed points), it follows that the eigenvalues of the Jacobian at the fixed point (17) of T^n are 1, -1, -1. Because the velocity-reversal property is only approximately satisfied, these values are not exact for finite n and m. However, they will be approached in the limit as $m\to\infty$.

This suggests that the special fixed point of T^n located at

$$x_c=0,\quad v_1=0,\quad v_2=-[2(r_n+1)/r_n]^{1/2}\ , \tag{18}$$

is a parabolic fixed point when viewed as a two-dimensional map of the surface of section into itself. Since any neighborhood of this point contains an infinite number of fixed points whose approximate locations are given by (17), it is not isolated and therefore its stability cannot be examined by linear stability analysis. The analogous fixed point in Lehtihet and Miller's problem[11] corresponds to the billiard dropping vertically right into the center of the wedge.

A second family of fixed points of T^n arises in the following way. Suppose the first BBC of the collision sequence occurs at $x_c=0$ with $|v_1|$ small and v_2 large and negative going into the collision. One can then imagine the map M of Eq. (14) being repeated n times in an infinitesimal time interval, after which the system emerges in the state $(x_c,-v_1,-v_2)$. Now if during the upper ball's rise and fall in time τ_2 the lower ball makes exactly m rises and falls, each of period τ_1, the condition $\tau_2=m\tau_1$ leads to the following fixed point (in which v_1 and v_2 are the velocities just before the first collision of the collision sequence):

$$\begin{aligned} x_c&=0\ ,\\ v_1&=\pm\left[\frac{2(r_n+1)}{m^2r_n+1}\right]^{1/2}\ ,\\ v_2&=-\left[\frac{2m^2(r_n+1)}{m^2r_n+1}\right]^{1/2}\ . \end{aligned} \tag{19}$$

Note that since $x_c=0$ throughout the collision sequence, there is no approximation involved in arriving at this result. Here too there is an infinite number of fixed points corresponding to integral values of m. The points lie along the v_2 axis of both the BBC Poincaré map and the $x_1=0$ Poincaré map for $r=r_n$. It is interesting to note that in the limit as $m\to\infty$, they approach the same special fixed point of T^n as that approached by the first family, namely the parabolic fixed point of Eq. (18).

VI. STRUCTURE OF THE POINCARÉ MAPS

Having located certain families of fixed points which exist when the mass ratio is equal to one of the r_n values, we are in a good position to understand the $x_1=0$ Poincaré maps for $r=r_n$. Later in this section we shall describe how the structure changes when r moves away from one of the r_n values.

Figures 3 and 4 are the $x_1=0$ Poincaré maps for $r_3=3.000$ and $r_4=5.828$. These were constructed in the following way. In each case the simple stable fixed point of Eq. (6) yields a fixed point on the x_2 axis, a little to the right of center. Surrounding this point are several regular curves which gradually change from approximately elliptical to a more and more distorted shape. Each of these curves was generated by 1000–4000 points using the following sets of initial values: v_{1c} set equal to $\bar{v}_{1c}$ of Eq. (6); x_c changed in increments of 0.1 from the value $\bar{x}_c$ given by Eq. (6); v_{2c} determined from energy conservation. Among these curves, the innermost curve of Fig. 4 consists of 23 islands, which failed to connect even when the trajectory had 10 000 points. In this case the initial values happened to generate an island chain of a kind known to be associated with the larger islands in the KAM theory. Other island chains of this nature will be described shortly.

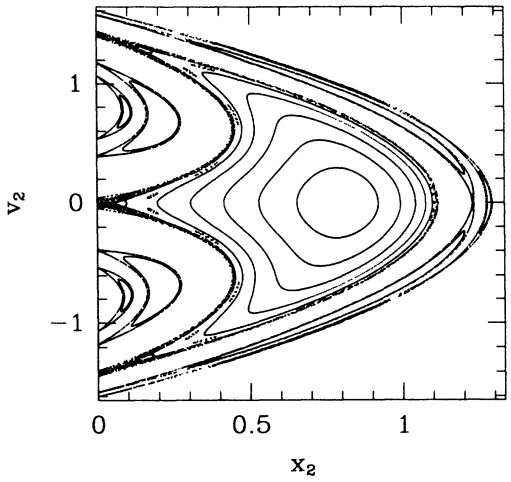

FIG. 3. $x_1=0$ Poincaré map for $r=r_3=3.000$, calculated as described in Sec. VI.

Outside the largest regular curve in Figs. 3 and 4 lies a chaotic region generated by setting $m=1$ in Eq. (19). (For computational reasons x_c was chosen to be 0.0001 and v_{1c} adjusted to conserve energy.) We shall call this the $m=1$ manifold. Setting $m=2$ and $m=3$ in Eq. (19) gives two additional chaotic regions, each of which consists of thin crescent-shaped outlines extending all the way to the v_2 axis, plus thin parabola-shaped regions around the outside, the $m=3$ region lying beyond the $m=2$ region. It is clear that the fixed points of Eq. (19)

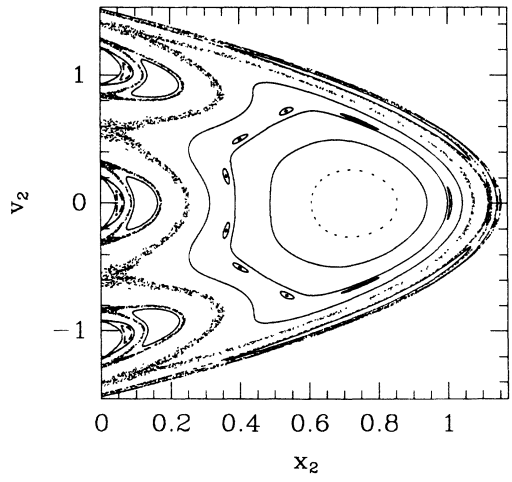

FIG. 4. $x_1=0$ Poincaré map for $r=r_4=5.828$, calculated as described in Sec. VI.

are unstable. It is also to be noted that the chaotic regions are not connected to each other.

Within the $m=2$ and 3 unstable manifolds lie island chains which were generated by setting $m=2$ and 3 in Eq. (17). These initial values gave islands rather than chains of fixed points because of the approximation of constant ball velocities between collisions of the n BBC sequence near $x=0$, which underlies Eq. (17). The actual fixed points lie inside these islands and are clearly stable fixed points. It can be seen in Fig. 3 that for $m=2$ there are four islands, while for $m=3$ there are five islands lying outside the four-island chain. A similar situation appears in Fig. 4: $m=2$ gives five islands while $m=3$ gives six islands lying outside the five-island chain.

The pattern of alternating regular and chaotic regions continues to be generated by assigning successively higher values to m in Eqs. (17) and (19). Figure 5 shows an enlargement of the region near $x_2=0$, $v_2=1.1$ of Fig. 4 obtained by setting $m=2,3,\ldots,10$. This beautiful interweaving of regular (stable) and chaotic (unstable) regions is similar to the behavior found in other nonlinear systems with two degrees of freedom.[1,6,9–11]

It remains to mention various island chains having no connection with Eqs. (17) and (19). An example is the chain of 13 islands in Fig. 3 lying between the $m=1$ unstable manifold and the largest regular curve. Another example is the chain of nine islands in Fig. 4 lying between the two largest regular curves. These are representative of many island chains that we have found by trial and error. In accordance with the KAM picture, we expect there are unstable (hyperbolic) fixed points between neighboring islands of each chain.

Close to the chaotic region generated by setting $m=1$ in Eq. (19) there are a number of related island chains which we now briefly describe. These are conveniently identified by their rotation numbers (Sec. III). For $r=r_3$ we have found island chains outside the largest regular curve but not embedded in the chaotic region with P/Q equal to 4/13, 9/29, 14/45, 19/61, 24/77, and 29/93.

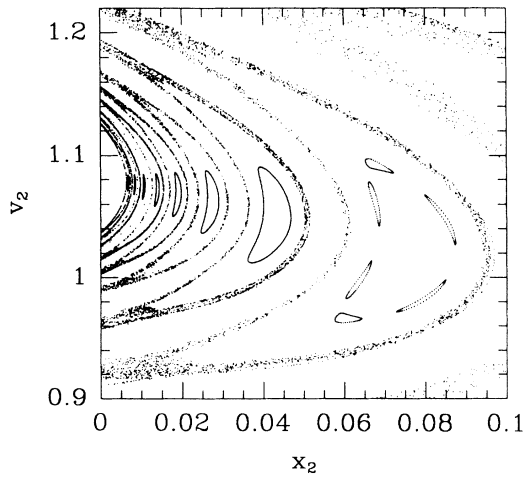

FIG. 5. Enlargement of the part of Fig. 4 near $x_2=0$, $v_2=1.1$. The cluster of six islands is visible in both figures.

Note that in each case the numerator increases by 5 while the denominator increases by 16. This does not continue indefinitely since we have found the 5/16 resonance lying embedded in the chaotic region. Thus the motion becomes unstable at a rotation number lying between $29/93=0.3118$ and $5/16=0.3125$. Similarly, for $r=r_4$ we have found interior island chains with P/Q equal to 2/9, 5/22, and 8/35. Here the numerator increases by 3 and the denominator by 13 in each case. However, we have also found the 3/13 island chain lying embedded in the chaotic region. Therefore the first unstable rotation number is somewhere between $8/35=0.2286$ and $3/13=0.2308$. Note that for both $r=r_3$ and r_4 the first unstable rotation number is close to $1/n$, the rotation number of the $m=1$ fixed point cycle given approximately by Eq. (19). It appears to be a general result that the first trajectory to become unstable on moving outward from the stable region lies very close to the $m=1$ unstable manifold.

Although we do not have a systematic way of generating the various island chains described in the preceding paragraph, we do know how to generate $r=r_n$ Poincaré maps such as Figs. 3 and 4. How do the plots change when r moves away from r_n? Some indication of what happens may be obtained by comparing Fig. 4 for $r=r_4=5.828$ with Fig. 2 calculated for $r=6.000$. Both figures used almost exactly the same sets of initial values. [The simple fixed point of Eq. (6) is at slightly different positions in the two figures.] The most striking difference is the fact that the entire chaotic region of Fig. 2 was generated by a single trajectory of 12 000 points; the many isolated chaotic regions of Fig. 4 have merged into a single unstable manifold. Another noteworthy feature is the appearance in Fig. 2 of four small "bumps" between the three main bumps of the $m=1$ unstable manifold of Fig. 4. These are probably associated with $n=5$ BBC sequences which become possible once r is greater than r_4. If r were increased beyond 6.000, these latter bumps would grow in size while the set of $n=4$ bumps would diminish. It is remarkable that so much of the structure of the Poincaré maps is connected in some way with the velocity-reversing collision sequences.

VII. MOTION IN THE LIMIT OF LARGE r

As the mass ratio r becomes large one might expect intuitively that the motion of the heavy ball would become like that of a single bouncing ball making elastic collisions with the floor. In other words, the very light lower ball might be expected to have a scarcely discernible effect on the upper ball's motion. This expectation is borne out by the calculations we have performed. However, instead of the upper ball making a single elastic collision with the floor, its velocity is reversed by means of numerous rapid collisions with the lower ball, which is trapped between the upper ball and the floor.

In Sec. IV we showed that for particular values r_n of the mass ratio, a rapid sequence of collisions involving n BBC's near $x=0$ has the effect of reversing the velocities of both balls. This mechanism appears to continue to

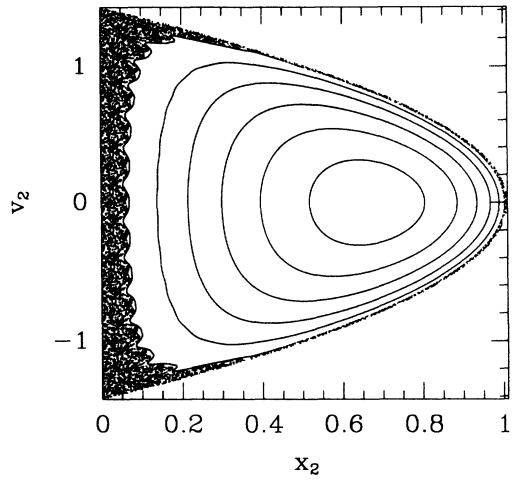

FIG. 6. $x_1=0$ Poincaré map for $r=100$.

operate in approximately the same way even when r is appreciably different from any of the r_n values.

Figure 6 shows the $x_1=0$ Poincaré section calculated for $r=100$. A prominent feature of this plot is the parabolic boundary which can be calculated by assuming all the energy of the system resides in the upper ball. From energy conservation one finds

$$v_2^2=2\frac{r+1}{r}-2x_2 , \tag{20}$$

which accurately describes the points on the outer boundary of the parabolic curve of the figure. The part of the figure for which x_2 is less than about 0.15 comes from the time interval during which the upper ball reverses its direction. There are 15 small peaks in this region, including the stretched-out peaks along the sides of the parabola. Now from Table I it can be seen that $r=100$ lies between $r_{15}=90.52$ and $r_{16}=103.09$. Since when $r=r_n$ there are $n-1$ peaks in the $x_1=0$ Poincaré section, it appears that the 15 peaks of the chaotic trajectory of Fig. 6 arise from approximately velocity-reversing collision sequences near $x=0$ involving 16 BBC's.

When r is large, Eq. (16) allows us to estimate the number of BBC's that are required to reverse the velocity of the upper ball. For large n we find,

$$n\approx\frac{\pi}{2}\sqrt{r} . \tag{21}$$

When $r=100$ this yields $n\approx 15.7$, implying $16-1=15$ peaks, as found in Fig. 6. For $r=1000$ it gives $n\approx 49.7$, which predicts $50-1=49$ peaks, in accord with the 49 peaks found on a plot similar to Fig. 6 for this case.

Equation (21) can be used to estimate, as a function of r, the width of the chaotic region bordering on the v_2 axis. Suppose an n BBC sequence begins at x_c, which we assume to be small, and let us further assume that just before the first BBC $v_1\approx 0$ while $|v_2|$ is large. After the first BBC, $|v_1|\approx 2|v_2|$ while $|v_2|$ is hardly changed by the collision. [See Eq. (13) for large r.] In this approximation the next BBC occurs at $x_c/3$. If the same approximations are made (with less and less justification at each step) it is not difficult to show that succeeding BBC's occur at $x_c/5$, $x_c/7$, and so on. In the same approximation scheme the positions of the points generated on the $x_1=0$ Poincaré map turn out to occur at $x_c/2$, $x_c/4$, $x_c/6$, and so on. Thus in the middle of the collision sequence the upper ball reaches its minimum position of $x_2^{\min}\approx x_c/2(n/2)=x_c/n$. Substituting for n from Eq. (21) and setting $x_c=1$ (an upper bound), we obtain

$$x_2^{\min}\approx\frac{2}{\pi}r^{-1/2} . \tag{22}$$

A comparison with Fig. 2 for $r=6$ shows that (22) gives a good estimate of the width of the chaotic region bordering the v_2 axis in this case. This suggests that the proportionality constant in Eq. (22) is about right, despite the unreliable way in which it was obtained. The interesting part of Eq. (22), however, is its dependence on $r^{-1/2}$. For $r=100$ this predicts the width of the chaotic region along the v_2 axis to be 0.064, in very good agreement with the calculated results of Fig. 6.

It is also possible to estimate the thickness of the parabola in the vicinity of $v_2=0$. It is easy to show that if the upper ball has all the energy in the system, it rises to a maximum height $x_2^{\max}=1+1/r$. The inner boundary of the chaotic parabola may be estimated by calculating the maximum height to which the upper ball rises while executing regular or stable motion. We have calculated this to be unity with an error of order $r^{-3/2}$. Thus $x_2^{\min}=1+O(r^{-3/2})$. Hence the spread in the points lying on the parabola at $v_2=0$ is $\Delta x_2=1/r+O(r^{-3/2})$. This estimate is in excellent agreement with the calculation of Fig. 6 for $r=100$.

From the preceding arguments, the area of the chaotic region of the $x_1=0$ Poincaré map is dominated at large r by the bumpy strip bordering the v_2 axis, the area of which is approximately $2\sqrt{2}x_2^{\min}\approx(4\sqrt{2}/\pi)r^{-1/2}$. Since the area enclosed by the parabola of Eq. (20) (in the limit of large r) is $4\sqrt{2}/3$, we estimate that the fraction of the accessible area of the Poincaré map occupied by the chaotic region is close to $1/\sqrt{r}$.

In the limit as $r\to\infty$, the chaotic region is predicted to disappear completely. This suggests that the limit of infinite r is an integrable case for the two-ball system. The corresponding situation for the billiard in the symmetric wedge is the limit $\theta\to 0$. Lehtihet and Miller[11] argued that the force acting on the billiard becomes purely radial in this limit and consequently the square of the angular momentum about the vertex is conserved. This additional conserved quantity makes the limit $\theta\to 0$ an integrable case. Using the canonical transformation[14] relating the two systems, we have determined that the corresponding conserved quantity in the two-ball system is $x_2^2(v_2-v_1)^2$.

There is another more physical way of obtaining this result. Except near the beginning and end of the collision sequence one has $v_1\gg v_2$, and in this regime the maximum height of the lower ball is just x_2, the position of the upper ball, which changes slowly. According to the Hamilton-Jacobi theory, the action integral for the lower

lower ball, $J_1 = 2m_1|v_1|x_2$, is conserved. Thus when $v_1 \gg v_2$, we have that $v_1^2 x_2^2$ is conserved, in agreement with the result of the preceding paragraph in the same regime. It may be noted that a similar argument involving the constancy of the action integral for the horizontal motion of the billiard in the symmetric wedge (in the regime $v_v\theta \ll v_h$, where v_v and v_h are the vertical and horizontal velocity components of the billiard) leads immediately to the magnitude of the angular momentum about the vertex being constant.

VIII. LYAPUNOV EXPONENTS

The method described in the Appendix enables one to calculate the Lyapunov exponents for any trajectory. The results may be expressed either in the form "per unit time" as in Eq. (A5) or "per collision" as in Eq. (A6). Since in the chaotic regime it is the collisions which cause neighboring trajectories to diverge, one might guess that the $\tilde{\lambda}_j$'s (per collision) have greater physical significance than the λ_j's (per unit time). This has been confirmed by our calculations. We have also found that when $\tilde{\lambda}_1$ is plotted as a function of the mass ratio, the resulting curve is smoother if $\tilde{\lambda}_1$ is taken per collision of either type rather than, say, per ball-ball collision. This perhaps reflects the fact that a nonlinear jolt occurs at every collision.

Because of the property expressed by Eq. (A7) it is sufficient to give results for $\tilde{\lambda}_1$ only. Figure 7 shows $\tilde{\lambda}_1$ calculated at 100 different values of r between 0 and 1. The solid curve results from following a trajectory until $\ln\gamma_1$ exceeded 100 (or until the number of ball-ball collisions exceeded 250), repeating this process 50 times while continuing along the same trajectory and then averaging the results. The error estimated from the standard deviation of these 50 calculated values is about 1%.

Also shown in Fig. 7 as the dashed curve is $\tilde{\lambda}_1(\bar{\xi})$ calculated for the fixed point $\bar{\xi}$ of Eq. (6). It was obtained by simply taking the natural logarithm of the modulus of the eigenvalue of the matrix $J(\bar{\xi})$ of Eq. (7) having the largest absolute value. (At a fixed point of the BBC Poincaré map, the time displacement matrix H of the Appendix is the same as the Jacobian matrix at the fixed point.) Although this curve comes from one very special periodic trajectory, it has the same shape as the solid curve and is in fairly good agreement with regard to the magnitude. Furthermore, using the fact that for the trajectory at $\bar{\xi}$ there is one floor-ball collision for every ball-ball collision and that $\tilde{\lambda}_1$ is defined as per collision of either type, it is not hard to show from Eq. (8) that $\tilde{\lambda}_1(\bar{\xi}) \approx r^{1/2}$ for small r, and that $\tilde{\lambda}_1(\bar{\xi}) \approx \frac{1}{2}(1-r)^{1/2}$ for r just less than unity. It is interesting that in addition to the square-root behavior, the numerical results in Fig. 7 show the asymmetry at $r=0$ and 1 due to the factor of $\frac{1}{2}$.

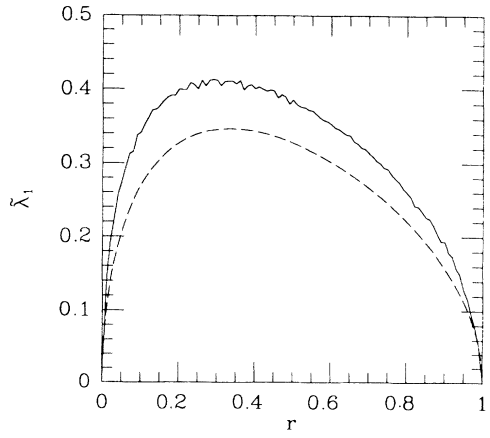

FIG. 7. The largest Lyapunov exponent $\tilde{\lambda}_1$ calculated at 100 values of r. Solid curve: calculated for chaotic trajectories by the method of the Appendix. Dashed curve: calculated at the fixed point $\bar{\xi}$ by taking the natural logarithm of the largest eigenvalue of the matrix $J(\bar{\xi})$ of Eq. (7).

The corresponding behavior for the billiard in the symmetric wedge studied by Lehtihet and Miller and by Miller and Ravishankar[11] may be obtained from [see Eq. (16)]

$$r = \cot^2\theta \ , \tag{23}$$

which relates the mass ratio r of the two balls to the semi-angle θ of the wedge. This relation follows from Wojtkowski's canonical transformation[14] relating the two-ball system of the present paper to the billiard in the symmetric wedge. Since $r=0$ corresponds to $\theta=\pi/2$ and $\cot(\pi/2-\eta) \approx \eta$ for small η, it follows from our results that $\tilde{\lambda}_1(\bar{\xi}) \approx \eta$ for $\theta = \pi/2 - \eta$. Likewise, since $r=1$ corresponds to $\theta=\pi/4$ and $\cot(\pi/4+\eta) \approx 1-2\eta$ for small η, our result for r just less than unity becomes $\tilde{\lambda}_1(\bar{\xi}) \approx \frac{1}{2}(4\eta)^{1/2} = \eta^{1/2}$. These exponents of 1 and 1/2 are precisely those found by Miller and Ravishankar[11] from both numerical studies and from a careful study of suitably averaged Jacobian matrices. Studies of similar two-dimensional billiard systems by Benettin[18] showed that as a parameter ε measuring the departure from the integrable case tends to zero, the largest Lyapunov exponent varies as $\varepsilon^{1/2}$, a result which has been proved rigorously for a particular case by Wojtkowski.[19] In the light of the above results it would appear that an appropriate choice for ε in the billiard problem of Ref. 11 is $|\cot^2\theta - \cot^2\theta_i|$ rather than $|\theta-\theta_i|$, where θ_i is either $\pi/2$ or $\pi/4$.

In Fig. 8 we show the results for $\tilde{\lambda}_1$ calculated for chaotic trajectories at 80 values of r between 1 and 5. This has the interesting feature that $\tilde{\lambda}_1$ appears to become small but nonzero near the point $r_3 = 3.00$. Figure 9 shows the results for $\tilde{\lambda}_1$ calculated at 190 values in the range $5 < r < 100$. The estimated numerical error at each point is approximately 5%. Here one finds minima close to the values $r_4 = 5.8$, $r_5 = 9.5$, $r_6 = 13.9$, $r_7 = 19.2$, $r_8 = 25.3$, $r_9 = 32.2$, $r_{10} = 39.9$, and so on. (See Table I.) We believe these minima in $\tilde{\lambda}_1$ result from the fact that the chaotic regions visible in Figs. 3–5 near the v_2 axis are not connected to each other. Consequently, any given chaotic trajectory is confined to a relatively small part of the phase space, and the exponential separation of initially close trajectories is thereby highly constrained.

There is another rather different way of explaining the minima at the r_n values. It was shown in Sec. IV that for $r = r_n$ the velocity-reversing collision sequences occurring near $x=0$ have the effect of preserving information about

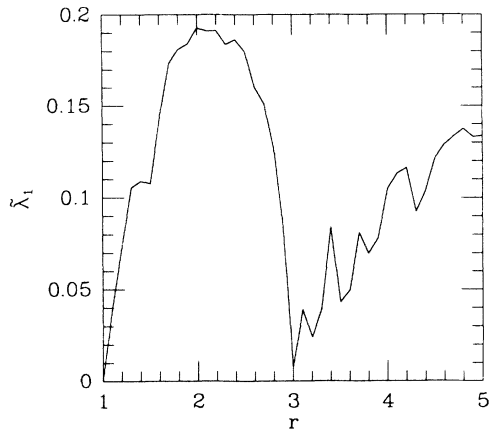

FIG. 8. The largest Lyapunov exponent $\tilde{\lambda}_1$ calculated at 80 values of r between 1 and 5 by the method described in the Appendix.

the system. It is likely that for long chaotic trajectories, such collision sequences will occur much more frequently when $r=r_n$ than when r is not close to one of the r_n values. Thus we expect the Kolmogorov entropy, which is a measure of how rapidly information about the system is lost, to decrease when r approaches one of the r_n values. The theorem of Pesin[16] relates the K entropy (or metric entropy) to the invariant measure of the flow and the sum of the positive Lyapunov exponents. Since for a Hamiltonian flow with two degrees of freedom there is at most one positive Lyapunov exponent, under suitable conditions one can write the metric entropy of the flow as[22]

$$h_\mu = \int_\Gamma \lambda(x) d\mu(x) \ . \tag{24}$$

Here $\lambda(x)$ is the positive Lyapunov exponent (written as a function of the trajectory's initial position in phase space), and the integral with respect to the invariant measure $\mu(x)$ in the chaotic region is taken over the constant energy manifold Γ. Since both $\lambda(x)>0$ and $\mu(x)>0$ in the chaotic region, a decrease in the K entropy at $r=r_n$ implies a decrease in either $\lambda(x)$ or $\mu(x)$ or both. This provides a plausible explanation of the results shown in Figs. 8 and 9.

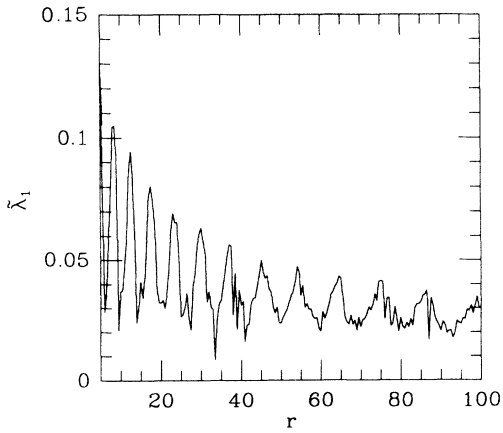

FIG. 9. The largest Lyapunov exponent $\tilde{\lambda}_1$ calculated at 190 values of r between 5 and 100 by the method described in the Appendix.

IX. CONCLUDING REMARKS

The two-ball system with discontinuities due to collisions exhibits complex dynamical behavior yet is simple enough that a great deal may be understood in physical terms. We have found that a central role is played by the velocity-reversing collision sequences occurring near $x=0$. While these are most sharply defined for particular values r_n of the mass ratio, they seem to occur, at least intermittently, for other values of r. The n BBC sequences near $x=0$ led to identifying families of stable and unstable fixed points which, together with the central elliptic fixed point and its invariant curves, largely determine the structure of the Poincaré maps for r greater than about 3. The infinite families of fixed points that we have identified have a common limit which we believe to be a parabolic fixed point.

It was mentioned in the Introduction that Wojtkowski[14] has shown that the two-ball system of the present paper is related by a canonical transformation to the billiard in a symmetric wedge studied by Lehtihet and Miller.[11] The simple relation (23) gives the correspondence between the mass ratio r in the two-ball system and the semiangle θ of the wedge. When $\theta>\pi/4$, Lehtihet and Miller found that "the motion is completely chaotic and suggests K-system behavior," just as we have found in the two-ball system for $r<1$. For the special case $\theta=\pi/4$ the motion of the billiard separates into two independent falling motions. This corresponds in our problem to the masses of the balls being equal ($r=1$). One can then regard the balls as passing through each other on collisions, giving essentially two independent motions. When $\theta<\pi/4$, Lehtihet and Miller found coexisting quasiperiodic and chaotic trajectories and the same kind of complex dynamical structure that we have found in the two-ball system for $r>1$.

When the wedge semiangle is equal to one of the values $\theta_n=\pi/(2n)$ for $n=3,4,\ldots$, Lehtihet and Miller, and Matulich and Miller[11] found that their Poincaré sections exhibited distinctive geometrical features. For the case $\theta=\pi/6$ they found their Poincaré section divided into infinitely many chaotic regions separated from each other by stable regions, instead of there being a single connected region of "global" chaos. Since $\theta=\pi/6$ corresponds to $r=r_3=3.00$ in the two-ball system, it is not surprising that we have found similar behavior in our Poincaré map for this case (Fig. 3). A similar situation probably prevails at each value of r_n and the corresponding angles θ_n for the wedge semiangle (for $n=3,4,\ldots$). Furthermore, as soon as one moves away from one of the r_n or θ_n values, it appears that in both systems the previously isolated chaotic regions merge together to form a single chaotic region. Judging from Figs. 2 and 4, this transition to global chaos appears to happen as soon as r differs

from r_n, although if the departure is very small it may take a long time for the trajectory to move from one previously isolated chaotic region to another.

We have presented an argument in Sec. VII showing that the measure of the chaotic region decreases as $r^{-1/2}$ as r increases. This suggests that the limit of infinite r (corresponding to the lower ball having zero mass) is an integrable case. Thus if the KAM theorem regarding the destruction of invariant tori remains valid for systems with discontinuities, it may be applicable for suitably large but finite values of r.

In contrast to this, Lehtihet and Miller argue that $\theta=\pi/4$, which corresponds to the two balls having equal masses, is an integrable case. To support their view they state that if θ is decreased below $\pi/4$, the measure of the chaotic regions gradually increases, and that "except for the presence of a small amount of global chaos, this behavior is similar to the perturbation of smooth systems for which the KAM theorem applies." We have confirmed that for $r=1.05$ the $x_1=0$ Poincaré map consists of a large number of island chains embedded in a sparse sea of global chaos. Thus, despite its peculiar nature, it may well be an integrable case to which the KAM theorem is relevant for $r>1$. However, as Lehtihet and Miller have noted, when θ is increased above $\pi/4$ (or r is decreased below unity), the motion abruptly changes from being integrable to being completely ergodic. This sudden change of behavior seems to rule out the possibility of applying the KAM theorem for $r<1$.

ACKNOWLEDGMENTS

We are grateful to Jack Wisdom for telling us about this problem. We also thank Tom Szeredi for useful discussions. This research was supported in part by the Natural Sciences and Engineering Research Council of Canada.

APPENDIX: CALCULATION OF THE LYAPUNOV EXPONENTS

In this appendix the method used to calculate the spectrum of Lyapunov exponents associated with a given trajectory is described. Our method is based on the work of Lorenz[20] and Greene and Kim.[21]

Consider a trajectory of the system between times t_0 and t_f. Normally one would think of the trajectory as the path $x_1(t),v_1(t),x_2(t),v_2(t)$ describing the time evolution of the system on the hypersurface of constant E. However, we have found it convenient to assume that the trajectory starts and ends with a ball-ball collision and to think of the motion as a sequence of mappings from one collision to the next. This allows us to choose the three independent variables to be x_c, v_{1c}, and v_{2c}, where x_c is the position of the colliding balls and v_{1c} and v_{2c} are the velocities of the balls immediately after the collision.

One now introduces a small departure $\delta(t_0)$ from the reference trajectory at time t_0 and calculates the resulting trajectory from t_0 to t_f. This trajectory ends up displaced from the reference trajectory by the vector $\delta(t_f)$. The time displacement matrix $H(t_f,t_0)$ is then defined by

$$\delta(t_f)=H\delta(t_0)\ . \tag{A1}$$

As Lorenz has indicated, an easy way to calculate the matrix H numerically is to choose $\delta(t_0)$ to be successively the column vectors $(\Delta x_c,0,0)^T$, $(0,\Delta v_{1c},0)^T$, and $(0,0,\Delta v_{2c})^T$, where T denotes the transpose. One can then subtract the numerical solution for the reference trajectory from the perturbed trajectory in each case, divide by the initial displacement and thus obtain the corresponding column of H. The matrix H has the property[21] that for any intermediate time t_i between t_0 and t_f,

$$H(t_f,t_0)=H(t_f,t_i)H(t_i,t_0)\ . \tag{A2}$$

The method of calculating the Lyapunov exponents from H has been clearly described by Lorenz.[20] A tiny sphere of departures from the initial point of the reference trajectory at time t_0 is given by

$$\delta^T(t_0)\delta(t_0)=\varepsilon^2\ . \tag{A3}$$

From Eq. (A1) this is carried into an ellipsoid at time t_f given by

$$\delta^T(t_f)(HH^T)^{-1}\delta(t_f)=\varepsilon^2\ . \tag{A4}$$

The lengths of the semiaxes of the ellipsoid are $\gamma_1\varepsilon,\gamma_2\varepsilon,\gamma_3\varepsilon$, where $\gamma_1,\gamma_2,\gamma_3$ are called the singular values of the matrix H. They are simply the positive square roots of the eigenvalues of HH^T or H^TH, and by convention are arranged so that $\gamma_1\geq\gamma_2\geq\gamma_3$. The key point is that while H is not a symmetric matrix, the product matrix HH^T or H^TH *is* symmetric and therefore has real eigenvalues, which, in fact, always turn out to be positive. Furthermore, the directions of the principal axes of the ellipsoid of Eq. (A4) are given by the eigenvectors of HH^T. Finally, the Lyapunov exponents are obtained by taking the limits

$$\lambda_j=\lim_{t_f\to\infty}\frac{\ln\gamma_j}{t_f-t_0}\ , \tag{A5}$$

assuming that the limits exist. Strictly speaking, the Lyapunov exponents pertain to a single trajectory starting from an initial point at t_0.

For reasons discussed in Sec. VIII we have found it useful to introduce a different set of Lyapunov exponents, defined per collision instead of per unit time:

$$\tilde{\lambda}_j=\lim_{N\to\infty}\frac{1}{N}\ln\gamma_j^{(N)}\ . \tag{A6}$$

Here N is the total number of collisions occurring between t_0 and t_f (not including the collision at time t_0), and the $\gamma_j^{(N)}$ are the singular values of the matrix $H(t_f,t_0)$.

The numerical problem of approximating the limits in Eqs. (A5) and (A6) is not at all straightforward. Under conditions such that the system exhibits chaotic behavior, the magnitude of the small departure $\delta(t)$ from the reference trajectory grows exponentially and soon becomes comparable with a typical dimension L of the volume of phase space in which the motion occurs. One way of proceeding would be to choose t_f in Eq. (A1) to be

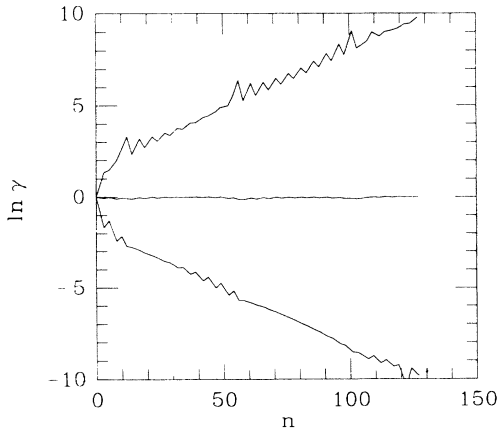

FIG. 10. Lyapunov exponent calculation for a chaotic trajectory for $r=0.99$. The natural logarithms of the three singular values are plotted against the total number of collisions n. The Lyapunov exponents are the slopes of the best-fitting straight lines.

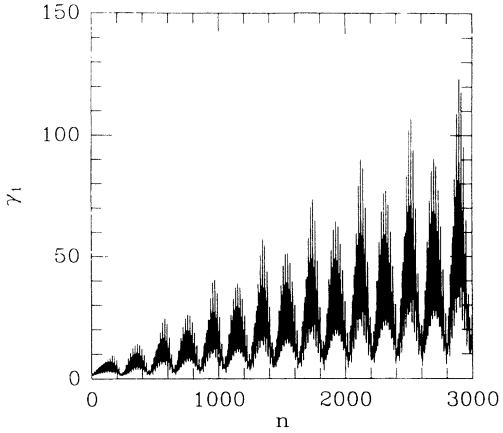

FIG. 11. Lyapunov exponent calculation for a quasiperiodic trajectory, the six-island chain of Fig. 2. The largest singular value γ_1 is plotted against the total number of collisions n. The fact that γ_1 grows linearly with n implies that the largest Lyapunov exponent is zero.

the time of the last collision for which $|\delta(t_f)|$ is less than, say, $0.001L$. One would then find the singular values of $H(t_f,t_0)$ and hence calculate estimates of λ_j and $\tilde{\lambda}_j$ from Eqs. (A5) and (A6), disregarding the limits. Good estimates for the λ_j and $\tilde{\lambda}_j$ would result from repeating this procedure many times over a long trajectory and averaging the results obtained.

We have found that a better approach is to make use of the property of the H matrix expressed by Eq. (A2). The matrix $H(t_n,t_{n-1})$ carrying the tiny displacement $\delta(t_{n-1})$ to the still tiny displacement $\delta(t_n)$ is calculated by the method described earlier. Equation (A2) is then used to calculate $H(t_n,t_0)$ from $H(t_{n-1},t_0)$. The singular values $\gamma_j^{(n)}$ of $H(t_n,t_0)$ are calculated and the values of $\ln\gamma_j^{(n)}$ are stored. Apart from questions of numerical accuracy (to be discussed below), there is no restriction on how large the singular values $\gamma_j^{(n)}$ may become. Carrying out this procedure for, say, 100 ball-ball collisions, we then perform a linear regression analysis on the set of values $\ln\gamma_j^{(n)}, n=1,\ldots,100$, plotted against either t_n-t_0 or the collision number n. We claim that the calculated value of the slope is a good estimate of λ_j or of $\tilde{\lambda}_j$. Repeating this entire procedure many times over a long trajectory and averaging the results leads to a reliable estimate for λ_j or $\tilde{\lambda}_j$.

A plot of the three different $\ln\gamma_j^{(n)}$ as a function of n is shown in Fig. 10 for a typical chaotic trajectory. The most striking feature of this figure is the fact that the slopes of the upper and lower curves (corresponding to $\tilde{\lambda}_1$ and $\tilde{\lambda}_3$) are very nearly equal and opposite while the slope of the middle curve (corresponding to $\tilde{\lambda}_2$) is close to zero. In fact the property

$$\lambda_3=-\lambda_1,\quad \lambda_2=0 \tag{A7}$$

is expected for any Hamiltonian system with two degrees of freedom on the basis of time reversal symmetry.[22] We have found $\tilde{\lambda}_1>0$, $\tilde{\lambda}_2=0$, and $\tilde{\lambda}_3=-\tilde{\lambda}_1$ for all chaotic trajectories studied. A similar result was demonstrated by Benettin, Galgani, and Strelcyn[22] for the Hénon-Heiles system. It should be added that Fig. 10 also shows the advantage of the linear regression analysis over simply taking $\ln\gamma_j^{(100)}/100$ to estimate $\tilde{\lambda}_j$. The first few collisions have the effect of introducing a nonzero intercept for the best-fitting straight line, and this affects the numerical value of the slope calculated from $\ln\tilde{\lambda}_1^{(100)}/100$ or $\ln\tilde{\lambda}_3^{(100)}/100$, as is evident from the diagram.

Figure 11 shows the results for $\gamma_1^{(n)}$ as a function of n calculated for a trajectory showing quasiperiodic rather than chaotic behavior. (In fact the initial point for Fig. 11 lies on an island similar to those found in Fig. 2.) Despite the spiky appearance of this graph, it is evident that on average $\gamma_1^{(n)}$ increases linearly with n. Thus it does not grow or decay exponentially and the corresponding Lyapunov exponent $\tilde{\lambda}_1$ is zero. From Eq. (A7) it follows that all three Lyapunov exponents are zero, a result which we have found to hold whenever the system exhibits quasiperiodic behavior. A similar result was found for quasiperiodic trajectories of the Hénon-Heiles system in Ref. 22.

Finally, we add a few comments about the numerical accuracy of the calculations. All calculations were performed in double precision arithmetic with an accuracy of about 16 digits. The main effect of this limited precision is that the smallest singular value γ_3 becomes numerically unreliable when the ratio γ_1/γ_3 is of the order of 10^{16}. This was checked by repeating a representative calculation in quadruple precision arithmetic, with the result that γ_3 became unreliable when $\gamma_1/\gamma_3\sim10^{31}$. To ensure that the correlation coefficient associated with the linear regression analysis is better than about 0.98, it was found to be necessary to allow the singular value γ_1 to grow until $\ln\gamma_1\sim50$. Since this was far beyond the point at which $\ln\gamma_3$ lost its numerical reliability, we then simply assumed that $\lambda_3=-\lambda_1$.

*Present address: Department of Physics, Yale University, New Haven, CT 06511.

†Present address: Department of Physics, Kenyon College, Gambier, OH 43022.

[1]M. Hénon and C. Heiles, Astrophys. J. **69**, 73 (1964).

[2]J. Ford, *Fundamental Problems in Statistical Mechanics,* edited by E. D. G. Cohen (North-Holland, Amsterdam, 1975), Vol. 3, p. 215.

[3]M. V. Berry, in *Topics in Nonlinear Dynamics, La Jolla, 1978,* Proceedings of the Workshop on Topics in Nonlinear Dynamics, AIP Conf. Proc. No. 46, edited by S. Jorna (AIP, New York, 1978), p. 16.

[4]B. V. Chirikov, Phys. Rep. **52**, 263 (1979).

[5]R. Z. Sagdeev, D. A. Usikov, and G. M. Zaslavsky, *Nonlinear Physics: From the Pendulum to Turbulence and Chaos* (Harwood, Chur, 1988).

[6]J. M. Greene, Physica D **18**, 427 (1986).

[7]Ya. G. Sinai, Russ. Math. Surv. **25** (2), 137 (1970).

[8]Ya. G. Sinai and N. I. Chernov, Russ. Math. Surv. **42** (3), 181 (1987).

[9]See the articles by A. Brahic, Astron. Astrophys. **12**, 98 (1971); and by M. A. Lieberman and A. J. Lichtenberg, Phys. Rev. A **5**, 1852 (1972), and references therein.

[10]G. Benettin and J.-M. Strelcyn Phys. Rev. A **17**, 773 (1978).

[11]H. E. Lehtihet and B. N. Miller, Physica D **21**, 93 (1986); B. N. Miller and K. Ravishankar, J. Stat. Phys. **53**, 1299 (1988); A. Matulich and B. N. Miller, Celestial Mech. **39**, 191 (1986).

[12]M. P. Wojtkowski, Commun. Math. Phys. **80**, 453 (1981).

[13]M. P. Wojtkowski, Commun. Math. Phys. **105**, 391 (1986).

[14]M. P. Wojtkowski, Commun. Math. Phys. **126**, 507 (1990).

[15]A. Katok and J.-M. Strelcyn, with the collaboration of F. Ledrappier and F. Przytycki, *Invariant Manifolds, Entropy and Billiards; Smooth Maps with Singularities,* Vol. 1222 of *Lecture Notes in Mathematics,* edited by A. Dold and B. Eckmann (Springer-Verlag, Berlin, 1986).

[16]Ya. B. Pesin, Russ. Math. Surv. **32** (4), 55 (1977).

[17]J. M. Greene, J. Math. Phys. **9**, 760 (1968).

[18]G. Benettin, Physica D **13**, 211 (1984).

[19]M. P. Wojtkowski, Ergod. Th Dyn. Syst. **8**, 133 (1988).

[20]E. N. Lorenz, Physica D **13**, 90 (1984).

[21]J. M. Greene and J.-S. Kim, Physica D **24**, 213 (1987).

[22]G. Benettin, L. Galgani, and J.-M. Strelcyn, Phys. Rev. A **14**, 2338 (1976).